Taylor & Francis
Taylor & Francis Group

Science and Technology of Advanced Materials: Methods

ISSN: (Print) (Online) Journal homepage: www.tandfonline.com/journals/tstm20

Autonomous search for half-metallic materials with *B*2 structure

Yuma Iwasaki, Ryo Toyama, Takahiro Yamazaki, Yasuhiko Igarashi, Masato Kotsugi & Yuya Sakuraba

To cite this article: Yuma Iwasaki, Ryo Toyama, Takahiro Yamazaki, Yasuhiko Igarashi, Masato Kotsugi & Yuya Sakuraba (2024) Autonomous search for half-metallic materials with *B*2 structure, Science and Technology of Advanced Materials: Methods, 4:1, 2403966, DOI: 10.1080/27660400.2024.2403966

To link to this article: https://doi.org/10.1080/27660400.2024.2403966

SCIENCE AND TECHNOLOGY OF ADVANCED MATERIALS: METHODS
2024, VOL. 4, NO. 1, 2403966
https://doi.org/10.1080/27660400.2024.2403966

Autonomous search for half-metallic materials with *B*2 structure

Yuma Iwasaki[a], Ryo Toyama[b], Takahiro Yamazaki[c], Yasuhiko Igarashi[d], Masato Kotsugi[c] and Yuya Sakuraba[b]

[a]Center for Basic Research on Materials (CBRM), National Institute for Materials Science (NIMS), Tsukuba, Japan; [b]Research Center for Magnetic and Spintronic Materials (CMSM), National Institute for Materials Science (NIMS), Tsukuba, Japan; [c]Department of Materials Science and Technology, Tokyo University of Science, Tokyo, Japan; [d]Graduate School of System and Information Engineering, University of Tsukuba, Tsukuba, Ibaraki, Japan

ABSTRACT

Exploring vast material spaces efficiently is challenging in materials science. Autonomous methods for material search – integrating machine learning and ab initio calculations – have emerged as powerful alternatives to traditional approaches, which are often time-consuming and limited in scope. Although these autonomous methods have been applied to various material systems, the extensive material space of *B*2 structured materials for half-metallicity remains largely unexplored. Herein, we introduce a simulation-based autonomous search approach to identify *B*2 structured alloys exhibiting high spin polarization of *sp* conduction electrons (P_{sp}), *sp* minority spin band gap (G_{sp}), and Curie temperature (T_c). The proposed method explores the material space of disordered quaternary *B*2 magnetic alloys using the Korringa – Kohn – Rostoker coherent potential approximation and Bayesian optimization. Over a continuous search of approximately 100 days, the system identified $Co_{1.0}Mn_{0.7}Al_{0.3}$ as a promising candidate, demonstrating high values of P_{sp}, G_{sp}, and T_c. Although additional experimental and theoretical validation is necessary, this study demonstrates the potential of autonomous material search methods to expedite material discovery and enhance material property optimization.

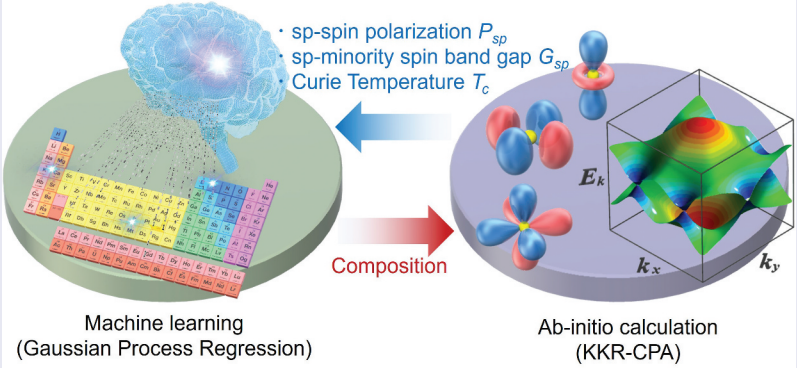

NOVELTY STATEMENT

Autonomous search methods identify a promising B2 structured alloy, $Co_{1.0}Mn_{0.7}Al_{0.3}$, with high spin polarization, minority spin band gap, and Curie temperature, showcasing a significant leap in efficient material discovery.

ARTICLE HISTORY
Received 24 July 2024
Revised 2 September 2024
Accepted 9 September 2024

KEYWORDS
Half-metal; machine learning; ab initio calculations; Bayesian optimization

Introduction

The scope of material spaces has recently expanded. Traditionally, humans have systematically explored these vast material spaces through iterative cycles of material synthesis, property measurement, and analysis. However, this traditional approach is time-consuming and inadequate for comprehensively exploring recently expanded material spaces. To overcome these limitations, researchers have integrated machine learning into automated material search methodologies. These approaches can be broadly categorized into two primary technologies: autonomous search based on robotics and material simulations. In the robotics approach, robots automate tasks such as material synthesis and property measurement. Subsequently, machine learning

CONTACT Yuma Iwasaki IWASAKI.Yuma@nims.go.jp Center for Basic Research on Materials (CBRM), National Institute for Materials Science (NIMS), Tsukuba, Japan
Supplemental data for this article can be accessed online at https://doi.org/10.1080/27660400.2024.2403966

analyzes the collected data to suggest materials and optimal process conditions for subsequent synthesis cycles. This closed-loop system – driven by robotic synthesis and measurement – enables autonomous material searches. With the development of numerous autonomous material search robots, robotic searching has emerged as a highly effective method in material development [1–12]. In the second approach, simulations – such as ab initio calculations – are used to obtain material property data. Subsequently, machine learning analyzes the data to guide future material design related to structure and composition. This iterative process forms a closed loop, enabling autonomous exploration of material spaces in a computer environment, offering convenience, versatility, and widespread adoption [13–20].

Herein, we describe simulation-based autonomous methods for exploring half-metallic materials with a $B2$ structure. Half-metallic materials are characterized by possessing a metallic spin band and a semiconducting spin band [21], which have been extensively investigated for applications in tunnel magnetoresistance (TMR) [22–25], giant magnetoresistance (GMR) [26–29], and other spintronic devices [30–32]. Heusler alloys are a promising category for half-metallic applications, often adopting $L2_1$ (X_2YZ) or $C1_b$ (XYZ) structures composed of three different elements: X, Y, and Z. Owing to their multielemental nature and disordered phases, the material search space for Heusler alloys is extensive, making simulation-based autonomous methods highly effective for exploration [14,19,33].

However, Heusler alloys present significant challenges in synthesis owing to their complex four-sublattice structures, often resulting in poor properties or synthesis failures despite promising predictions from machine learning and ab initio calculations. The high synthesis temperatures required for Heusler alloys are a bottleneck for practical device applications. In contrast, the $B2$ structure is simpler, featuring only two sublattices, and can be viewed as a disordered form of the $L2_1$ structure, making it more feasible to synthesize at lower temperatures. In fact, half-metallicity in B2-structured materials such as Co_2(MnFe)Ge, Co_2MnGe, Co_2MnSi, and Co_2(CrFe)Al has been studied from experimental and theoretical perspectives [34–40]. Therefore, suggesting material compositions with potential half-metallicity in the $B2$ structure through autonomous material search methods is promising for successful synthesis and practical application.

Methods

The material space was defined as quaternary $B2$ materials with two sublattices: A site composed of two disordered elements (A^1 and A^2), and B site composed of two disordered elements (B^1 and B^2). The composition at each site was incremented by 10 atomic percent (at%). Therefore, the composition formula for the materials under exploration is expressed as

$$A^1_{1-a}A^2_aB^1_{1-b}B^2_b,$$

where A, B, a, and b are defined as

$$A^1, A^2 = \{Li, Mg, Ti, V, Mn, Fe, Co, Ni, Cu, Ru, Rh, Pd, Ag, Cd, Ir, Pt, Au\},$$

$$B^1, B^2 = \left\{ \begin{array}{c} Li, Be, B, Mg, Al, Si, Sc, Ti, V, Cr, Mn, Fe, Co, Ni, Cu, Zn, Ga, Ge, As, Y, Zr \\ Nb, Mo, Ru, Ag, In, Sn, Sb, La, Ce, Nd, Pr, Nd, Sm, Gd, Tb, Dy, Ho, Er, \\ Tm, Yb, Lu, Pt, Pb \end{array} \right\}$$

and

$$a, b = \{0, 0.1, 0.2, 0.3, 0.4, 0.5, 0.6, 0.7, 0.8, 0.9, 1.0\}.$$

The elements A^1 and A^2 predominantly occupy the X site in $L2_1$ structures (X_2YZ), whereas B^1 and B^2 typically reside at the Y or Z sites [41]. To reduce the number of candidate materials, the exploration was intentionally limited to materials containing Fe, Co, or Ni, which are major magnetic elements at room temperature. This approach narrowed the scope to approximately 4.4 million potential material configurations in the specified material space. The challenge of performing ab initio calculations for all candidates was alleviated using sequential calculations guided by machine learning, which efficiently navigated the material space.

The autonomous search simultaneously maximizes three indicators. The first indicator is sp spin polarization (P_{sp}). Typically, spin polarization is defined as the difference in the density of states (DOS) between up- and down-spin electrons at the Fermi level. Higher spin polarization values are linked to increased magnetoresistance (MR) ratios in TMR and GMR devices. However, studies have demonstrated that the MR ratio is more influenced by the spin polarization of conduction electrons (sp) than the total electron (spd) spin polarization [24,33,36,42].

$$P_{sp} = \frac{n_{sp}^{\uparrow}(E_F) - n_{sp}^{\downarrow}(E_F)}{n_{sp}^{\uparrow}(E_F) + n_{sp}^{\downarrow}(E_F)},$$

where $n_{sp}^{\uparrow}(E_F)$ and $n_{sp}^{\downarrow}(E_F)$ are the DOS of up- and down-spin electrons at the Fermi level, respectively.

The second indicator is the *sp* minority spin band gap (G_{sp}). When P_{sp} is high and approaches 1.0, the DOS of *sp* minority spin electrons at the Fermi level is nearly zero, indicating the existence of an *sp* minority spin band gap. A larger G_{sp} indicates that half-metallicity remains stable even at room temperature, preventing the formation of electronic states in the *sp* minority spin band gap.

The third indicator is Curie temperature (T_c), which is the temperature at which a magnetic material transitions from a magnetic to a nonmagnetic state. A higher T_c indicates more stable magnetic properties, which is critical for spintronic device applications.

The methodology for autonomous material search is depicted in Figure 1. It includes sequential ab initio calculations and machine learning. The ab initio phase calculates P_{sp}, G_{sp}, and T_c based on compositions recommended by the machine learning phase. Data accumulated from these calculations guide the composition choices for subsequent ab initio calculations.

The ab initio calculations used Green's function-based density functional theory using the Korringa – Kohn – Rostoker coherent potential approximation (KKR – CPA) method, implemented in AkaiKKR software [43]. CPA allows accurate simulations of alloy systems, particularly for multielement disordered phases [44–47]. P_{sp} and G_{sp} were determined from the DOS, whereas T_c was calculated using the following equation:

$$T_c = \frac{2}{3}\frac{(E_{fmg} - E_{lmd})}{ck_B},$$

where E_{fmg} and E_{lmd} are the total energies of the ferromagnetic and local moment disorder states, respectively [48], k_B is the Boltzmann constant, and c is the concentration of magnetic atoms. The lattice constants were optimized to minimize the total energy. Further details of the ab initio calculations are provided in the Supplementary Materials (S1).

The machine learning phase used Bayesian optimization [49] and an autoencoder [50] to identify material compositions for subsequent KKR – CPA calculations based on accumulated T_c data. The material space (descriptors) was designed based on a previous report [19]. A composition vector and Magpie descriptor vector [51] were compressed into a 30-dimensional latent vector representing the unexplored material space. Additional details are provided in the Supplementary Materials (S2). This phase integrated KKR – CPA with multiobjective Bayesian optimization, using P_{sp}, G_{sp}, and T_c as objective variables and the latent vectors generated by the autoencoder as explanatory variables in the Gaussian-process regression model. The upper confidence bound (UCB) was calculated as an acquisition function for each material [52]. The candidate material with the highest Pareto hypervolume, based on the UCB value and training data (observed P_{sp}, G_{sp}, and T_c), was selected for subsequent KKR – CPA calculations. This iterative approach facilitated autonomous exploration for materials exhibiting high P_{sp}, G_{sp}, and T_c. Further details are provided in the Supplementary Materials (S3).

Results and Discussion

The developed autonomous search system operated continuously for approximately 100 days. Figure 2(a) depicts a three-dimensional plot of the explored

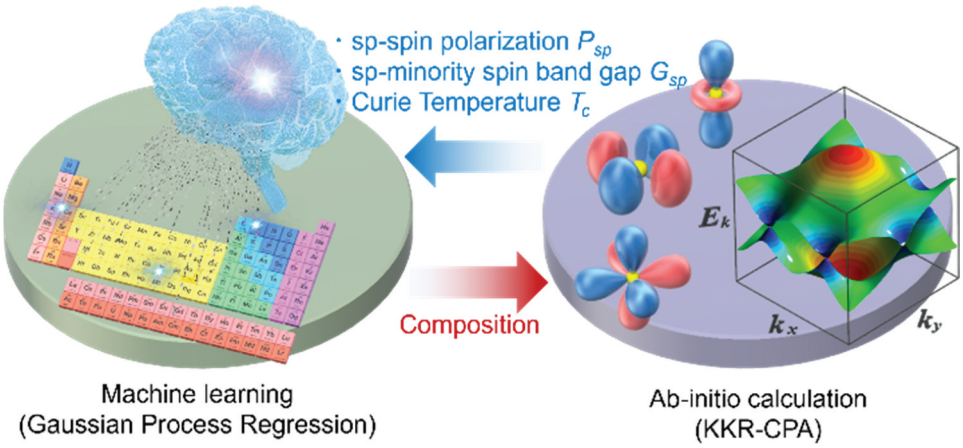

Figure 1. Overview of an autonomous material search system; the *ab initio* calculation phase computes *sp* spin polarization (P_{sp}), *sp* minority spin band gap (G_{sp}), and Curie temperature (T_c) using crystal structure and composition data determined in the machine learning phase; the machine learning phase generates compositional information for subsequent *ab initio* calculations (KKR – CPA = korringa – Kohn – Rostoker coherent potential approximation). This method is based on previous research [19].

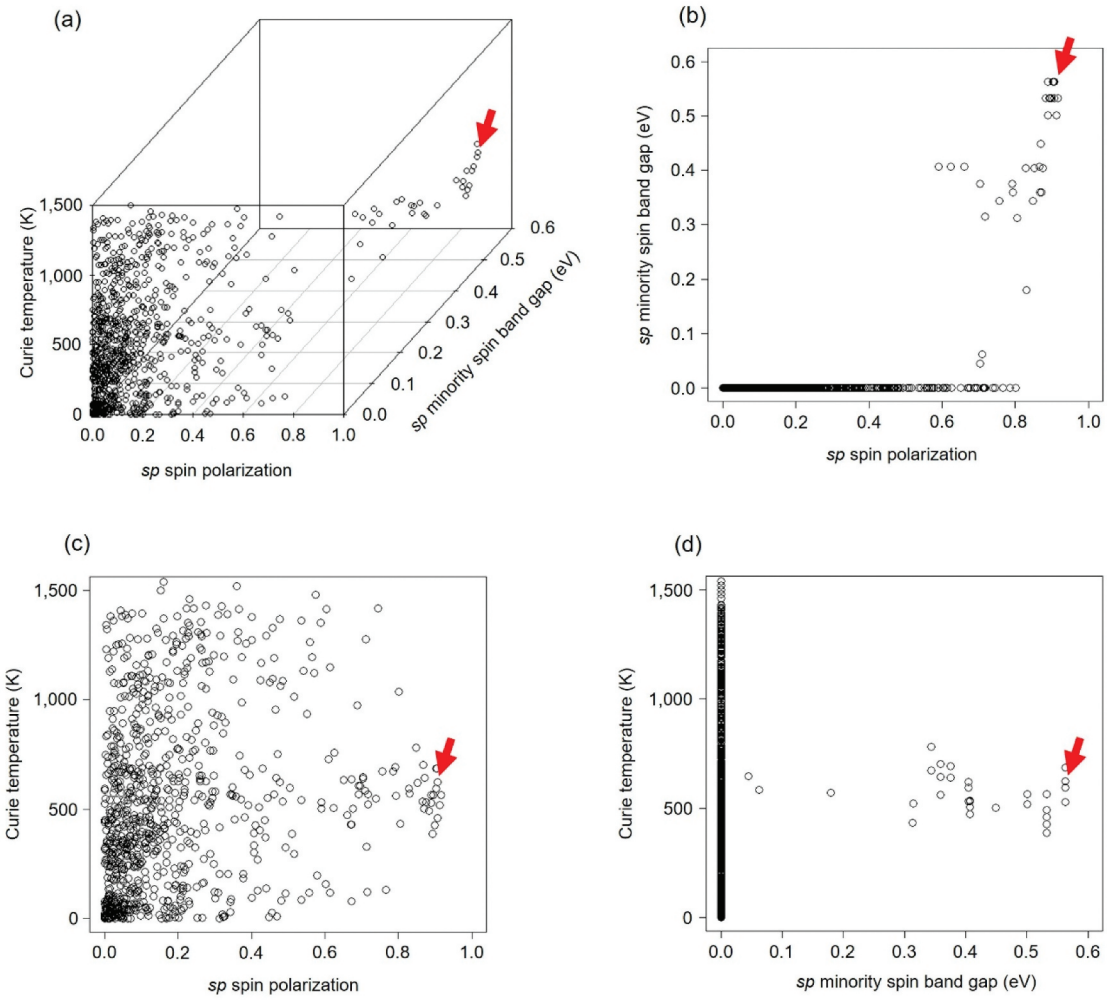

Figure 2. Results of the autonomous search for materials with high *sp* spin polarization (P_{sp}), *sp* minority spin band gap (G_{sp}), and Curie temperature (T_c); (a) three-dimensional plot of the materials explored by the system, illustrating their P_{sp}, G_{sp}, and T_c; (b) two-dimensional plot of P_{sp} vs. G_{sp}; (c) two-dimensional plot of P_{sp} vs. T_c; (d) two-dimensional plot of G_{sp} vs. T_c. Red arrows show *B*2-$Co_{1.0}Mn_{0.7}Al_{0.3}$.

materials, illustrating their P_{sp}, G_{sp}, and T_c characteristics. For clarity, Figures 2(b–d) show two-dimensional plots of P_{sp} vs. G_{sp}, P_{sp} vs. T_c, and G_{sp} vs. T_c. Materials with low P_{sp} typically lack a minority spin band gap, resulting in a G_{sp} value of zero. Although some materials showed potential for very high Curie temperatures (T_c >1,000 K), these data points are speculative because the stability of the *B*2 structure at such high temperatures is uncertain.

Despite adopting the *B*2 structure, several new alloys with high P_{sp}, G_{sp}, and T_c were proposed. One such alloy is *B*2-$Co_{1.0}Mn_{0.7}Al_{0.3}$ shown by red arrows in Figure 2(a–d). A well-known half-metallic material composed of Co, Mn, and Al is the full-Heusler alloy $L2_1$-$Co_{2.0}Mn_{1.0}Al_{1.0}$, which demonstrates high magnetic moments, spin polarization, and Curie temperatures, making it highly promising for applications in TMR and GMR devices [53]. However, the synthesis of $L2_1$-$Co_{2.0}Mn_{1.0}Al_{1.0}$ is challenging, often resulting in the formation of *B*2-$Co_{2.0}Mn_{1.0}Al_{1.0}$ instead, attributed to the low order/disorder transition temperature [54–56].

The proposed *B*2-$Co_{1.0}Mn_{0.7}Al_{0.3}$ alloy is predictably more promising than $L2_1$-$Co_{2.0}Mn_{1.0}Al_{1.0}$ and *B*2-$Co_{2.0}Mn_{1.0}Al_{1.0}$. Figures 3(a–c) depict the crystal structures of *B*2-$Co_{1.0}Mn_{0.7}Al_{0.3}$, *B*2-$Co_{2.0}Mn_{1.0}Al_{1.0}$, and $L2_1$-$Co_{2.0}Mn_{1.0}Al_{1.0}$, respectively. These figures, generated using VESTA software [57], show Co in yellow, Mn in red, and Al in blue, with disorder observed in the Mn and Al sites for *B*2-$Co_{1.0}Mn_{0.7}Al_{0.3}$ and *B*2-$Co_{2.0}Mn_{1.0}Al_{1.0}$. Figures 3(d–f) display the total DOS, encompassing all *spd* orbitals, for *B*2-$Co_{1.0}Mn_{0.7}Al_{0.3}$, *B*2-$Co_{2.0}Mn_{1.0}Al_{1.0}$, and $L2_1$-$Co_{2.0}Mn_{1.0}Al_{1.0}$ and indicating high spin polarization across all materials. Figures 3(g–i) depict the DOS specifically for conduction electron *sp* orbitals, crucial for GMR and TMR devices. All materials exhibit pronounced *sp* spin polarization and minority spin band gap-like features, with *B*2-$Co_{1.0}Mn_{0.7}Al_{0.3}$ displaying a particularly sharp minority spin band gap edge.

Table 1 presents the magnetic moment (*M*), lattice constant (*a*), *sp* spin polarization (P_{sp}), *sp* minority spin band gap (G_{sp}), Curie temperature (T_c), and formation energy (ΔEf) for *B*2-$Co_{1.0}Mn_{0.7}Al_{0.3}$, *B*2-$Co_{2.0}$

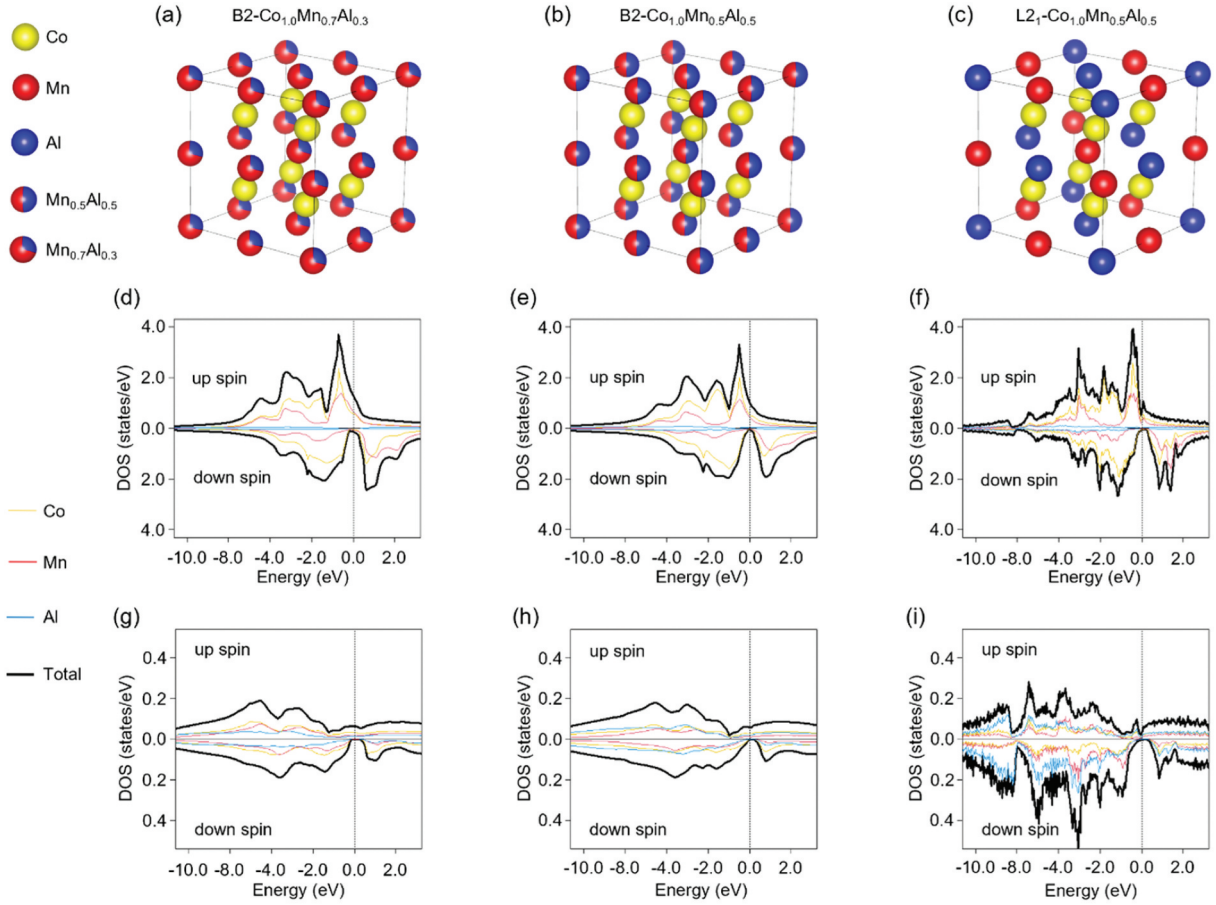

Figure 3. Density of states (DOS) of *B*2-$Co_{1.0}Mn_{0.7}Al_{0.3}$, *B*2-$Co_{2.0}Mn_{1.0}Al_{1.0}$, and $L2_1$-$Co_{2.0}Mn_{1.0}Al_{1.0}$; (a) crystal structure of *B*2-$Co_{1.0}Mn_{0.7}Al_{0.3}$; (b) crystal structure of *B*2-$Co_{2.0}Mn_{1.0}Al_{1.0}$; (c) crystal structure of $L2_1$-$Co_{2.0}Mn_{1.0}Al_{1.0}$; (d) total (*spd*) electron DOS of *B*2-$Co_{1.0}Mn_{0.7}Al_{0.3}$; (e) total (*spd*) electron DOS of *B*2-$Co_{2.0}Mn_{1.0}Al_{1.0}$; (f) total (*spd*) electron DOS of $L2_1$-$Co_{2.0}Mn_{1.0}Al_{1.0}$; (g) conduction (*sp*) electron DOS of *B*2-$Co_{1.0}Mn_{0.7}Al_{0.3}$; (h) conduction (*sp*) electron DOS of *B*2-$Co_{2.0}Mn_{1.0}Al_{1.0}$; (i) conduction (*sp*) electron DOS of $L2_1$-$Co_{2.0}Mn_{1.0}Al_{1.0}$.

Table 1. Magnetic moment (*M*), lattice constant (*a*), *sp* spin polarization (P_{sp}), *sp* minority spin band gap (G_{sp}), Curie temperature (T_c), and formation energy (ΔEf) for *B*2-$Co_{1.0}Mn_{0.7}Al_{0.3}$, *B*2-$Co_{2.0}Mn_{1.0}Al_{1.0}$, and $L2_1$-$Co_{2.0}Mn_{1.0}Al_{1.0}$ calculated by KKR – CPA.

	M (μ_B)	a (Å)	P_{sp}	G_{sp} (eV)	T_c (K)	ΔEf (eV/cell)
B2-$Co_{1.0}Mn_{0.7}Al_{0.3}$	1.41	2.801	0.913	0.563	620.732	−0.74856
B2-$Co_{1.0}Mn_{0.5}Al_{0.5}$	1.023	2.806	0.906	0.344	411.337	−1.34266
$L2_1$-$Co_{2.0}Mn_{1.0}Al_{1.0}$	1.03	5.619	0.744	0.313	587.613	−2.68496

$Mn_{1.0}Al_{1.0}$, and $L2_1$-$Co_{2.0}Mn_{1.0}Al_{1.0}$. These values were calculated using the KKR – CPA method used in the autonomous search, with detailed calculation conditions provided in Supplementary Materials (S1). The P_{sp}, G_{sp}, and T_c values for the newly proposed *B*2-$Co_{1.0}Mn_{0.7}Al_{0.3}$ surpass those of the well-known *B*2-$Co_{2.0}Mn_{1.0}Al_{1.0}$ and $L2_1$-$Co_{2.0}Mn_{1.0}Al_{1.0}$, highlighting the effectiveness of the autonomous search system in identifying promising new materials.

The newly proposed *B*2-$Co_{1.0}Mn_{0.7}Al_{0.3}$ (*B*2-$Co_{2.0}Mn_{1.4}Al_{0.6}$) can be regarded as a significantly different material from $L2_1$-$Co_{2.0}Mn_{1.0}Al_{1.0}$ in terms of the stoichiometric composition as its composition is rich in Mn and poor in Al and perfect disorder between Mn and Al atoms. Note that, in previous experimental and theoretical studies, a lot of effort has been made to enhance spin polarization by controlling compositions deviating from the stoichiometric composition of an ideal $L2_1$ structure. For instance, materials with compositions deviating from $L2_1$ structures in the Co_2MnSi, $Co_2Mn(Ge,Ga)$, and $Co_2(Mn,Fe)Si$ systems have been investigated [42,58,59]. The MR ratio in TMR and GMR devices is improved by relatively reducing the Co composition ratio from the stoichiometric one, which is reflected in the reduction in the number of Co anti-sites, a major cause of reduced spin polarization. However, *B*2-$Co_{1.0}Mn_{0.7}Al_{0.3}$ proposed by our autonomous material search is considered a new single material with high spin polarization originating from a mechanism different from the suppression of Co anti-sites in the previously studied Co-poor $L2_1$ structure as the proposed material has the *B*2

structure and stoichiometric Co composition ratio. The fact that it has a disordered $B2$ structure, which is easier to synthesize than $L2_1$, adds practical value.

Machine learning analysis, particularly white-box approaches, may help deduce material mechanisms in the future. Although extracting valuable insights from data accumulated through the autonomous material search may be challenging due to significant data bias, supplementing the database with high-throughput ab initio calculations and experiments can eventually provide new data-driven insights into the material mechanisms.

Herein, we successfully used autonomous exploration methods to propose new $B2$ alloys with high P_{sp}, G_{sp}, and T_c. However, these newly proposed alloy materials are speculative predictions derived from ab initio calculations, and the accuracy of P_{sp}, G_{sp}, and T_c predictions has not been verified. Moreover, the stability of the disordered $B2$ structure formed by the elements in these alloys is uncertain. Notably, a negative formation energy does not necessarily guarantee synthesizability, necessitating further experimental and theoretical investigations of the proposed alloy materials.

Conclusions

A simulation-based autonomous material search method is highly effective in exploring the extensive alloy space of quaternary $B2$ materials, focusing on achieving high *sp* spin polarization (P_{sp}), *sp* minority spin band gap (G_{sp}), and Curie temperature (T_c). By integrating machine learning and ab initio calculations, this system efficiently navigates the complex material landscape, ultimately proposing the new material $Co_{1.0}Mn_{0.7}Al_{0.3}$ with exceptional P_{sp}, G_{sp}, and T_c values. This autonomous search approach demonstrates versatility and adaptability across various material systems and properties, serving as a powerful tool capable of accelerating advancements in material discovery.

Acknowledgements

We thank K. Masuda and K. Sodeyama at the National Institute for Materials Science. This study was supported by JST-CREST Grant JPMJCR21O1.

Disclosure statement

No potential conflict of interest was reported by the authors.

Funding

This study was supported by JST-CREST under Grant [JPMJCR21O1]; Core Research for Evolutional Science and Technology [JPMJCR21O1].

ORCID

Yuma Iwasaki http://orcid.org/0000-0002-7117-277X
Ryo Toyama http://orcid.org/0000-0002-7398-5803
Takahiro Yamazaki http://orcid.org/0000-0003-0738-9373
Yasuhiko Igarashi http://orcid.org/0000-0003-1042-6657
Masato Kotsugi http://orcid.org/0000-0002-4841-1808
Yuya Sakuraba http://orcid.org/0000-0003-4618-9550

Data availability statement

The data supporting the results of this research are available from the corresponding author upon reasonable request.

References

[1] Coley CW, Thomas DA, Lummiss JA, et al. A robotic platform for flow synthesis of organic compounds informed by AI planning. Science. 2019;365(6453):eaax1566. doi: 10.1126/science.aax1566
[2] Burger B, Maffettone PM, Gusev VV, et al. A mobile robotic chemist. Nature. 2020;583(7815):237–241. doi: 10.1038/s41586-020-2442-2
[3] Nikolaev P, Hooper D, Webber F, et al. Autonomy in materials research: a case study in carbon nanotube growth. NPJ Comput Mater. 2016;2(1):16031. doi: 10.1038/npjcompumats.2016.31
[4] Shimizu R, Kobayashi S, Watanabe Y, et al. Autonomous materials synthesis by machine learning and robotics. APL Mater. 2020;8(11):111110. doi: 10.1063/5.0020370
[5] Li Z, Najeeb MA, Alves L, et al. Robot-accelerated perovskite investigation and discovery. Chem Mater. 2020;32(13):5650–5663. doi: 10.1021/acs.chemmater.0c01153
[6] Roch LM, Häse F, Kreisbeck C, et al. ChemOS: orchestrating autonomous experimentation. Sci Robot. 2018;3(19):eaat5559. doi: 10.1126/scirobotics.aat5559
[7] Attia PM, Grover A, Jin N, et al. Closed-loop optimization of fast-charging protocols for batteries with machine learning. Nature. 2020;578(7795):397–402. doi: 10.1038/s41586-020-1994-5
[8] Granda JM, Donina L, Dragone V, et al. Controlling an organic synthesis robot with machine learning to search for new reactivity. Nature. 2018;559(7714):377–381. doi: 10.1038/s41586-018-0307-8
[9] Szymanski NJ, Zeng Y, Huo H, et al. Toward autonomous design and synthesis of novel inorganic materials. Mater Horiz. 2021;8(8):2169–2198. doi: 10.1039/D1MH00495F
[10] Ren Z, Ren Z, Zhang Z, et al. Autonomous experiments using active learning and AI. Nat Rev Mater. 2023;8(9):563–564. doi: 10.1038/s41578-023-00588-4
[11] Szymanski NJ, Rendy B, Fei Y, et al. An autonomous laboratory for the accelerated synthesis of novel materials. Nature. 2023;624(7990):86–91. doi: 10.1038/s41586-023-06734-w
[12] Tamura R, Tsuda K, Matsuda S. NIMS-OS: an automation software to implement a closed loop between artificial intelligence and robotic experiments in materials science. Sci Technol Adv Mater. 2023;3(1):2232297. doi: 10.1080/27660400.2023.2232297

[13] Iwasaki Y, Sawada R, Saitoh E, et al. Machine learning autonomous identification of magnetic alloys beyond the Slater-Pauling limit. Commun Mater. 2021;2(1):31. doi: 10.1038/s43246-021-00135-0
[14] Sawada R, Iwasaki Y, Ishida M. Boosting material modeling using game tree search. Phys Rev Mater. 2018;2(10):103802. doi: 10.1103/PhysRevMaterials.2.103802
[15] Seko A, Togo A, Hayashi H, et al. Prediction of low-thermal-conductivity compounds with first-principles anharmonic lattice-dynamics calculations and bayesian optimization. Phys Rev Lett. 2015;115(20):205901. doi: 10.1103/PhysRevLett.115.205901
[16] Jalem R, Kanamori K, Takeuchi I, et al. Bayesian-driven first-principles calculations for accelerating exploration of fast ion conductors for rechargeable battery application. Sci Rep. 2018;8(1):5845. doi: 10.1038/s41598-018-23852-y
[17] Kusaba A, Kangawa Y, Kuboyama T, et al. Exploration of a large-scale reconstructed structure on GaN(0001) surface by Bayesian optimization. Appl Phys Lett. 2022;120(2):021602. doi: 10.1063/5.0078660
[18] Furuya D, Miyashita T, Miura Y, et al. Autonomous synthesis system integrating theoretical, informatics, and experimental approaches for large-magnetic-anisotropy materials. Sci Technol Adv Mater: Meth. 2022;2(1):280–293. doi: 10.1080/27660400.2022.2094698
[19] Iwasaki Y, Hwang J, Sakuraba Y, et al. Efficient autonomous material search method combining ab initio calculations, autoencoder, and multi-objective Bayesian optimization. Sci Technol Adv Mater: Meth. 2022;2(1):365–371. doi: 10.1080/27660400.2022.2123263
[20] Hwang J, Iwasaki Y. Improving efficiency of autonomous material search via transfer learning from non-target properties. Sci Technol Adv Mater: Meth. 2023;3(1):2254202. doi: 10.1080/27660400.2023.2254202
[21] Elphick K, Frost W, Samiepour M, et al. Heusler alloys for spintronic devices: review on recent development and future perspectives. Sci Technol Adv Mater. 2021;22(1):235–271. doi: 10.1080/14686996.2020.1812364
[22] Sakuraba Y, Hattori M, Oogane M, et al. Giant tunneling magnetoresistance in Co_2MnSi/Al–O/Co_2MnSi magnetic tunnel junctions. Appl Phys Lett. 2006;88(19):192508. doi: 10.1063/1.2202724
[23] Liu H, Honda Y, Taira T, et al. Giant tunneling magnetoresistance in epitaxial Co_2MnSi/MgO/Co_2MnSi magnetic tunnel junctions by half-metallicity of Co_2MnSi and coherent tunneling. Appl Phys Lett. 2012;101(13):132418. doi: 10.1063/1.4755773
[24] Moges K, Honda Y, Liu H, et al. Enhanced half-metallicity of off-stoichiometric quaternary Heusler alloy Co_2(Mn,Fe)Si investigated through saturation magnetization and tunneling magnetoresistance. Phys Rev B. 2016;93(13):134403. doi: 10.1103/PhysRevB.93.134403
[25] Shan R, Sukegawa H, Wang WH, et al. Demonstration of half-metallicity in fermi-level-tuned heusler alloy $Co_2FeAl_{0.5}Si_{0.5}$ at room temperature. Phys Rev Lett. 2009;102(24):246601. doi: 10.1103/PhysRevLett.102.246601
[26] Iwase T, Sakuraba Y, Bosu S, et al. Large interface spin-asymmetry and magnetoresistance in fully epitaxial Co_2MnSi/Ag/Co_2MnSi current-perpendicular-to-plane magnetoresistive devices. Appl Phys Express. 2009;2(6):063003. doi: 10.1143/APEX.2.063003
[27] Takahashi YK, Srinivasan A, Varaprasad B, et al. Large magnetoresistance in current-perpendicular-to-plane pseudospin valve using a $Co_2Fe(Ge_{0.5}Ga_{0.5})$ Heusler alloy. Appl Phys Lett. 2011;98(15):152501. doi: 10.1063/1.3576923
[28] Sakuraba Y, Ueda M, Miura Y, et al. Extensive study of giant magnetoresistance properties in half-metallic Co_2(Fe,Mn)Si-based devices. Appl Phys Lett. 2012;101(25):252408. doi: 10.1063/1.4772546
[29] Jung JW, Sakuraba Y, Sasaki TT, et al. Enhancement of magnetoresistance by inserting thin NiAl layers at the interfaces in $Co_2FeGa_{0.5}Ge_{0.5}$/Ag/$Co_2FeGa_{0.5}Ge_{0.5}$ current-perpendicular-to-plane pseudo spin valves. Appl Phys Lett. 2016;108(10):102408. doi: 10.1063/1.4943640
[30] Kimura T, Hashimoto N, Yamada S, et al. Room-temperature generation of giant pure spin currents using epitaxial Co_2FeSi spin injectors. NPG Asia Mater. 2012;4(3):e9. doi: 10.1038/am.2012.16
[31] Seki T, Sakuraba Y, Arai H, et al. High power all-metal spin torque oscillator using full Heusler Co_2(Fe,Mn)Si. Appl Phys Lett. 2014;105(9):092406. doi: 10.1063/1.4895024
[32] Bosu S, Sepehri-Amin H, Sakuraba Y, et al. High frequency out-of-plane oscillation with large cone angle in mag-flip spin torque oscillators for microwave assisted magnetic recording. Appl Phys Lett. 2017;110(14):142403. doi: 10.1063/1.4979324
[33] Kurniawan I, Miura Y, Hono K. Machine learning study of highly spin-polarized Heusler alloys at finite temperature. Phys Rev Mater. 2022;6(9):L091402. doi: 10.1103/PhysRevMaterials.6.L091402
[34] Nakatani T, Mihajlovic G, Read JC, et al. High signal output in current-perpendicular-to-the-plane giant magnetoresistance sensors using In–Zn–O-based spacer layers. Appl Phys Express. 2015;8(9):093003. doi: 10.7567/APEX.8.093003
[35] Nakatani T, Li S, Sakuraba Y, et al. Advanced CPP-GMR spin-valve sensors for narrow reader applications. IEEE Trans Magn. 2018;54(2):1–11. doi: 10.1109/TMAG.2017.2753221
[36] Li S, Nakatani T, Masuda K, et al. Enhancement of current-perpendicular-to-plane giant magnetoresistive outputs by improving B2-order in polycrystalline $Co_2(Mn_{0.6}Fe_{0.4})Ge$ Heusler alloy films with the insertion of amorphous CoFeBTa underlayer. Acta Materialia. 2018;142:49–57. doi: 10.1016/j.actamat.2017.09.046
[37] Picozzi S, Continenza A, Freeman AJ. Role of structural defects on the half-metallic character of Co_2MnGe and Co_2MnSi Heusler alloys. Phys Rev B. 2004;69(9):094423. doi: 10.1103/PhysRevB.69.094423
[38] Miura Y, Nagao K, Shirai M. Atomic disorder effects on half-metallicity of the full-Heusler alloys $Co_2Cr_{1-x}Fe_xAl$: a first-principles study. Phys Rev B. 2004;69:144413. doi: 10.1103/PhysRevB.69.144413
[39] Miura Y, Shirai M, Nagao K. First-principles study on half-metallicity of disordered $Co_2Cr_{1-x}Fe_xAl$. J Appl Phys. 2004;95(11):7225–7227. doi: 10.1063/1.1669115
[40] Özdog˘an K, Galanakis I. Effect of order on the half-metallic gap in Heusler compounds. J Appl Phys. 2011;110(7):076101. doi: 10.1063/1.3642990

[41] Yin M, Hasier J, Nash P. A review of phase equilibria in Heusler alloy systems containing Fe, Co or Ni. J Mater Sci. 2016;51(1):50–70. doi: 10.1007/s10853-015-9389-y
[42] Li G, Honda Y, Liu H, et al. Effect of nonstoichiometry on the half-metallic character of Co_2MnSi investigated through saturation magnetization and tunneling magnetoresistance ratio. Phys Rev B. 2014;89(1):014428. doi: 10.1103/PhysRevB.89.014428
[43] Akai KKR (machikaneyama). Ab-initio electronic-structure calculation code. Available from: http://kkr.issp.u-tokyo.ac.jp
[44] Akai H. Electronic structure Ni-Pd alloys calculated by the self-consistent KKR-CPA method. J Phys Soc Jpn. 1982;51(2):468–474. doi: 10.1143/JPSJ.51.468
[45] Khan SN, Staunton JB, Stocks GM. Statistical physics of multicomponent alloys using KKR-CPA. Phys Rev B. 2016;93(5):054206. doi: 10.1103/PhysRevB.93.054206
[46] Yang L, Liu B, Luo H, et al. Investigation of the site preference in Mn_2RuSn using KKR-CPA-LDA calculation. J Magn Mater. 2015;382(15):247–251. doi: 10.1016/j.jmmm.2015.01.081
[47] Akai H. Fast Korringa-Kohn-Tostoker coherent potential approximation and its application to FCC Ni-Fe systems. J Phys: Condens Matter. 1989;1(43):8045–8064. doi: 10.1088/0953-8984/1/43/006
[48] Akai H, Dederichs PH. Local moment disorder in ferromagnetic alloys. Phys Rev B Condens Matter. 1993;47(14):8739–8747. doi: 10.1103/PhysRevB.47.8739
[49] Snoek J, Larochelle H, Adams RP. Practical bayesian optimization of machine learning algorithms. Adv Neural Inf Process Syst. 2012;25:2960–2968.
[50] Hinton GE, Salakhutdinov RR. Reducing the dimensionality of data with neural networks. Science. 2006;313(5786):504–507. doi: 10.1126/science.1127647
[51] Ward L, Agrawal A, Choudhary A, et al. A general-purpose machine learning framework for predicting properties of inorganic materials. NPJ Comput Mater. 2016;2(1):16028. doi: 10.1038/npjcompumats.2016.28
[52] Auer P. Using confidence bounds for exploitation-exploration trade-off. J Mach Learn Res. 2002;3:397–422.
[53] Ishida S, Fujii S, Kashiwagi S, et al. Search for half-metallic compounds in Co2MnZ (Z=iiib, IVb, vb element). J Phys Soc Jpn. 1995;64(6):2152–2157. doi: 10.1143/JPSJ.64.2152
[54] Kubota H, Nakata J, Oogane M, et al. Large magnetoresistance in magnetic tunnel junctions using Co-mn-al full Heusler alloy. Jpn J Appl Phys. 2004;43(7B):L984. doi: 10.1143/JJAP.43.L984
[55] Sakuraba Y, Nakata J, Oogane M, et al. Magnetic tunnel junctions using B2-ordered Co2MnAl Heusler alloy epitaxial electrode. Appl Phys Lett. 2006;88(2):022503. doi: 10.1063/1.2162867
[56] Zhu X, Jiang E, Dai Y, et al. Stability, magnetic, and electronic properties of L21 and B2 phases in Co_2MnAl Heusler alloy. J Alloys Compd. 2015;632:528–532. doi: 10.1016/j.jallcom.2015.01.198
[57] Momma K, Izumi F. VESTA 3 for three-dimensional visualization of crystal, volumetric and morphology data. J Appl Crystallogr. 2011;44(6):1272–1276. doi: 10.1107/S0021889811038970
[58] Liu H, Kawami T, Moges K, et al. Influence of film composition in quaternary Heusler alloy Co_2(Mn,Fe)Si thin films on tunnelling magnetoresistance of Co_2(Mn,Fe)Si/MgO-based magnetic tunnel junctions. J Phys D: Appl Phys. 2015;48(16):164001. doi: 10.1088/0022-3727/48/16/164001
[59] Li S, Takahashi YK, Sakuraba Y, et al. Large enhancement of bulk spin polarization by suppressing CoMn anti-sites in $Co_2Mn(Ge_{0.75}Ga_{0.25})$ Heusler alloy thin film. Appl Phys Lett. 2016;108(12):122404. doi: 10.1063/1.4944719